공학석사 학위논문

Investigation of atomic and electronic structures of $LaAlO_3/Sr_xCa_{1-x}TiO_3/SrTiO_3$ interfaces using Cs-corrected STEM and EELS

2015년 8월

서울대학교 대학원

공과대학 재료공학부

손운배

Abstract

Investigation of atomic and electronic structures of $LaAlO_3/Sr_xCa_{1-x}TiO_3/SrTiO_3$ interfaces using Cs-corrected STEM and EELS

Woonbae Sohn

Department of Materials Science and Engineering

College of Engineering

Seoul National University

Two dimensional electron gas (2DEG) has got an intense interest since it was discovered in the $LaAlO_3/SrTiO_3$ interface in 2004. Many researches were carried out to reveal the origin of the 2DEG but there is not any established theory. On the other hand, in the year 2013, there is a report about electrical properties of $LaAlO_3/Sr_xCa_{1-x}TiO_3/SrTiO_3$. In this report, as the composition of Sr increases, the interfacial conductivity increases by 6 order of magnitude. Difference in the degree of TiO_6 octahedral tilt was suggested as the origin of the difference in electrical properties of the interfaces. The research is motivated by this report.

In this work, atomic and electronic structures of the $LaAlO_3/CaTiO_3/SrTiO_3$ and $LaAlO_3/SrTiO_3$ were investigated using Cs corrected TEM and EELS. Each samples showed same tendency in sheet

resistance as that of the previous report. High resolution HAADF and ABF STEM images showed that $CaTiO_3$ has considerable degree of octahedral rotation whereas we could hardly observe octahedral rotation at the $SrTiO_3$ substrate in $LaAlO_3/SrTiO_3$ system. However, considerable amount of Ti^{3+} was detected in both samples. From this, we concluded that regardless of the portion of Ti^{3+} at the interface, TiO_6 octahedral tilt angle plays a crucial role determining interfacial conductivity. To generalize this statement, we will try the same procedure in the $LaAlO_3/Sr_{0.5}Ca_{0.5}TiO_3/SrTiO_3$ system.

Keywords : Two Dimensional Electron Gas, Cs corrected transmission electron microscope, octahedral tilt, perovskite oxide

Student Number : 2013-20605

Contents

Chapter 1 Introduction

1.1 Transitional metal oxide in perovskite structure

1.2 Complex oxide interfaces and 2 Dimensional Electron Gas

1.3 Origin of 2DEG : Hypotheses

1.4 Motivation

1.5 Goal of this work

Chapter 2 Experimental Method

2.1 TEM sample preparation

2.2 Film characterization

2.3 TEM characterization

Chapter 3 Results and Discussions

3.1 Reproducibility of the $LaAlO_3/Sr_xCa_{1-x}TiO_3/SrTiO_3$ system

3.2 Atomic-scale observation of the $LaAlO_3/Sr_xCa_{1-x}TiO_3/SrTiO_3$ interfaces

3.3 Investigation of the electronic structures at the interfaces (EELS)

Chapter 4 Conclusions

Chapter 5 References

List of Tables

Table 1.1 List of conductivity of $CaTiO_3$, $Sr_{0.5}Ca_{0.5}TiO_3$ and $SrTiO_3$ at the room temperature

Table 3.1. Sheet resistance of $LaAlO_3/CaTiO_3/SrTiO_3$ and $LaAlO_3/SrTiO_3$ structure (units : Ω). Comparison with the reference [10] is included.

Table 3.2 Distribution, size of the two type of grains in the polycrystalline $CaTiO_3$ film

Table 3.3 Peak position of L_2, L_3 (in eV) and L_3/L_2 intensity ratio in the $LaAlO_3/CaTiO_3/SrTiO_3$ and $LaAlO_3/SrTiO_3$ structure. Each positions are marked in the HAADF STEM image as shown in Fig 3.9.

List of Figures

Fig 1.1 Schematic illustration of (a) cubic and (b) BO_6 octahedral tilted ABO_3 perovskite structure. Bonds between B site cation and O anion are described as polyhedrons.

Fig 1.2 Schematic description of a 2DEG at the $LaAlO_3/SrTiO_3$ interface. 2DEG in oxide interface was firstly discovered by Othomo and Hwang.

Fig 1.3 Polarization catastrophe model for atomically sharp (001) interfaces between $LaAlO_3$ and $SrTiO_3$. (a) The unreconstructed interface has neutral (001) planes in $SrTiO_3$, but the (001) planes in $LaAlO_3$ have alternating net charges (ρ). If the interface plane is $AlO_2/LaO/TiO_2$, this produces a non-negative electric field (E), leading in turn to an electric potential (V) that diverges with thickness. (b) If the interface is placed at the $AlO_2/SrO/TiO_2$ sequence instead, the potential negatively diverges. (c) The divergence of electrical potential at the $AlO_2/LaO/TiO_2$ interface can be avoided if half an electron is added to the last Ti layer. **(d)** Polarization catastrophe $AlO_2/SrO/TiO_2$ interface can also be avoided by removing half an electron from the SrO plane in the form of oxygen vacancies.

Fig 1.4 Schematic description of the electronic reconstruction at the (a) $AlO_2/LaO/TiO_2$ and (b) $AlO_2/SrO/TiO_2$ interface. (c) Intensity profile showing the fractions of Ti and La from the Ti L and La M edges at the $AlO_2/LaO/TiO_2$ interface. Ti^{3+} fraction was determined from a least-squares fit to the Ti-L edge from Ti^{3+} and Ti^{4+} reference spectra. There is excess Ti^{3+} on the substrate side of the interface (d) Corresponding Ti and La EELS profiles for the $AlO_2/SrO/TiO_2$

interface, showing almost no excess Ti^{3+}

Fig 1.5. (a) Aberration – corrected HAADF image of a 10-uc $SrTiO_3$/1-ML LaO film grown on $SrTiO_3$. The rectangular box represents the region of EELS line scans. (b) EELS spectra of Ti-L_2, L_3 and O-K edges obtained from line scans across the interface shown in (a). The spacing along the line scan between consecutive EELS spectra is 2.8 Å. The spectra at the LaO layer are highlighted by thicker lines. For the spectra for Ti L_2 and L_3 edges, peak broadening and less pronounced peak splitting at the interface are clearly observed. (c) HAADF images of 10-uc $SrTiO_3$/1-ML LaO/$SrTiO_3$ and 10-uc $SrTiO_3$/1-ML SmO/$SrTiO_3$ heterostructures. Both samples show no obvious defects or dislocations, indicating coherent interfaces. (d) Selected area Ti-L_2, L_3 EELS spectra obtained at the interfaces for 10-uc $SrTiO_3$/1-ML LaO/$SrTiO_3$ and 10-uc $SrTiO_3$/1-ML SmO/$SrTiO_3$ heterostructures. The arrow is a guide for comparison.

Fig 1.6 Density of states and structural relaxation of 3.5-uc SrTiO3/1-ML LaO (A and C) periodic superlattice and 3.5-uc $SrTiO_3$/1-ML YO periodic superlattice (B and D) obtained from DFT calculations. Positive density of states is for spin up and negative is for spin down. The dashed line indicates the position of the Fermi level. The results indicate conducting behavior for the 3.5-uc $SrTiO_3$/1-ML LaO periodic superlattice and insulating behavior for the 3.5-uc $SrTiO_3$/1-MLYO periodic superlattice.

Fig 1.7 (a) HRTEM image of a $LaAlO_3$/$CaTiO_3$/$SrTiO_3$ structure. The inset is the FFT patterns from the $CaTiO_3$ layer. HRTEM images of (b) $LaAlO_3$/$CaTiO_3$ and (c) $CaTiO_3$/ $SrTiO_3$ interfaces showing the sharp interface indicated by red arrows. (d) SAED pattern of the $LaAlO_3$/$CaTiO_3$/$SrTiO_3$ structure. (e) Phase contrast TEM

images and (f) SAED pattern of a $LaAlO_3/Sr_{0.5}Ca_{0.5}TiO_3/SrTiO_3$ structure. (12-1) weak spot was detected in the pattern.

Fig 1.8 (a) Typical I-V curves of $LaAlO_3$ (5 nm)/$Sr_xCa_{1-x}TiO_3$ (10 nm)/$SrTiO_3$ structures. For comparison, I-V curves of $LaAlO_3/SrTiO_3$ and bulk $SrTiO_3$ are presented. (b) Current at 5V and sheet conductance of the $LaAlO_3/SrxCa_{1-x}TiO_3/SrTiO_3$ structures as a function of atomic composition of Sr. As the composition of Sr increased, sheet conductance increased by 6 orders of magnitude.

Fig 1.9 Schematic illustration of TiO_6 octahedron in cubic (a) $SrTiO_3$ and orthorhombic (b) $CaTiO_3$. Octahedral rotations in $CaTiO_3$ are highlighted by the Ti-O-Ti angle much lower than 180 degrees. This is because ionic radius of Ca is smaller than Sr, leading to lower the tolerance factor, 't'.

Fig 2.1 Schematic diagram of the TEM sample preparation using polishing and precision ion milling (a) Thin film specimen is glued to another. (b) After curing, the whole specimen was sectioned. (c) Sectioned specimen is polished until its thickness gets under 10μm. (d) After the thinned specimen is separated from the pyrex holder, it is glued to molybdenum slot grid. (f) Top view of the specimen with the Mo grid. Finally, the specimen was thinned using PIPS system.

Fig 2.2 Schematic illustration of STEM. Depending on the electron scattering angle, HAADF, ADF, BF and LAADF STEM image can be obtained.

Fig 2.3 Core loss spectra acquired from the reference sample Ti^{3+} from LaTiO3 and Ti^{4+} from SrTiO3 with the same specimen thickness and same experimental conditions

Fig 3.1. AFM images of a (a) $LaAlO_3/CaTiO_3/SrTiO_3$ and (b) $LaAlO_3/SrTiO_3$

structures.

Fig 3.2 (a) ABSF – filtered Cross-sectional HRTEM image of the $LaAlO_3/CaTiO_3/SrTiO_3$ structure on the $[010]_p$ zone axis. $CaTiO_3$ film was grown in polycrystalline. (b) FFT diffraction patterns from the region 1 of the $CaTiO_3$ layer. (c) FFT diffraction patterns from the region 2 of the $CaTiO_3$ layer. (d) ABSF – filtered Cross-sectional HRTEM image of the $LaAlO_3/SrTiO_3$ structure on the [010] zone axis. $LaAlO_3$ film was epitaxially grown on $SrTiO_3$ substrate. The LaAlO3/SrTiO3 interface looks sharp.

Fig 3.3 Projection of $CaTiO_3$ atomic unit cell on the (a) $[100]_p$ and (b) $[001]_p$ zone axis using ball and stick model

Fig 3.4 Simulated HR image of stoichiometric $CaTiO_3$ on the $[100]_p$ zone axis. Stripe pattern is not observed in the simulated image.

Fig 3.5 Cs corrected high resolution HAADF STEM image of (a) $LaAlO_3/CaTiO_3/SrTiO_3$ and (b) $LaAlO_3/SrTiO_3$ structures. Interfaces are atomically sharp in both.

Fig 3.6 (a) HAADF STEM image of the $CaTiO_3$ film. (b) $[100]_p$ projection of the CaTiO3 film. Image (a) is observed in this projection. (c) Simulated HAADF image of the $CaTiO_3$ film. This well matches with the experimental image.

Fig 3.7 Aberration corrected high resolution ABF STEM image of (a) $LaAlO_3/CaTiO_3/SrTiO_3$ and (b) $LaAlO_3/SrTiO_3$ structures. Octahedral tilt has been observed in the $CaTiO_3$ film whereas there is not any octahedral rotation in the $SrTiO_3$ substrate in the $LaAlO_3/SrTiO_3$ structure. Each atomic columns are marked

as colored circles.

Fig 3.8 (a) High Resolution ABF STEM image of the $LaAlO_3/CaTiO_3/SrTiO_3$ structure. Ti-O-Ti angle had been measured by averaging all of the angles in the same line. The number of the lines are denoted in the image. (b) Average angle distribution of the $CaTiO_3$ film. Error bars are correspond to standard deviation.

Fig 3.9 (a) HAADF STEM image, (b) Ti L edge and (c) O K edge of the $LaAlO_3/CaTiO_3/SrTiO_3$ structure. (d) HAADF STEM image,(e) Ti L edge and (f) O K edge of the $LaAlO_3/SrTiO_3$ structure.

Fig 3.10. Ti L edge at the (a) $LaAlO_3/CaTiO_3$ and (b) $LaAlO_3/SrTiO_3$ interface. Both interfaces contain Ti^{3+} ions. Ratio of Ti^{3+} at the $LaAlO_3/CaTiO_3$ interface is higher than that of $LaAlO_3/SrTiO_3$ interface because $CaTiO_3$ is grown in non-stoichiometric condition. Ti^{3+} was observed not only at the interface but whole the $CaTiO_3$ film.

Chapter 1. Introduction

1.1. Transitional metal oxide in perovskite structure

Researches related to ABO_3 perovskite compounds have been of a great interest among scientists and engineers. This is mainly because perovskite oxides have a wide range of physical properties, related to many possible applications such as memory devices.

Perovskite oxides was first discovered in 1839 by Gustav Rose, who gave the name of Russian mineralogist L. Perovski to the $CaTiO_3$ compound. Nowadays, perovskite structure has been observed in non-oxide metal-organic compounds such as $(CH_3NH_3)PbI_3$. In this sense, perovskite structure refers to the ABX_3 compounds where X is not necessarily oxygen.

In the case of cubic ABO_3 perovskite structure, the A cation is located at the corner of the cube and B cation is located at the body center of the cube. Oxygen anions are located at the face center of the cube, hence oxygen anions form an octahedron as shown in Fig 1.1. This ideal cubic structure can be viewed of alternating AO and BO_2 planes when ABO_3 is viewed on the [100] zone axis.

However, cubic structure of perovskite is an ideal case and generally, perovskite oxides have tetragonal, orthorhombic, monoclinic or rhombohedral structures. The type of lattice structure is governed by the so-called the Goldschmidt tolerance factor,

$$t = \frac{r_A + r_B}{\sqrt{2}(r_B + r_O)} \qquad (1.1.1)$$

where r_A, r_B and r_O are the ionic radii of A, B and O respectively.[1] If t is equal or

almost 1, ABO_3 becomes cubic like $SrTiO_3$ and $BaZrO_3$. On the other hand, if t is less than 1, or the radius A-site cations become smaller, A cation cannot fill the available space in the lattice. BO_6 octahedron then tends to rotate to occupy as much space as possible in the lattice. This lowers crystal symmetry of the perovskite oxide.

Using the tolerance factor, effect of strain on octahedral rotation can be explained although there is not term related to the lattice constant in 't'. Consider the perovskite film which is in-plane strained on the perovskite substrate. If the film is compressively strained, even if the size of cations are small, there is more available space where A site cation can be filled. Thus, octahedral tilt angle is gets smaller and the rotation is suppressed. Conversely, if the perovskite compound is tensile strained, in-plane lattice constant becomes larger. To occupy space as much as possible, BO_6 octahedron is much more rotated and oxygen anions tend to be closer to A site cations.

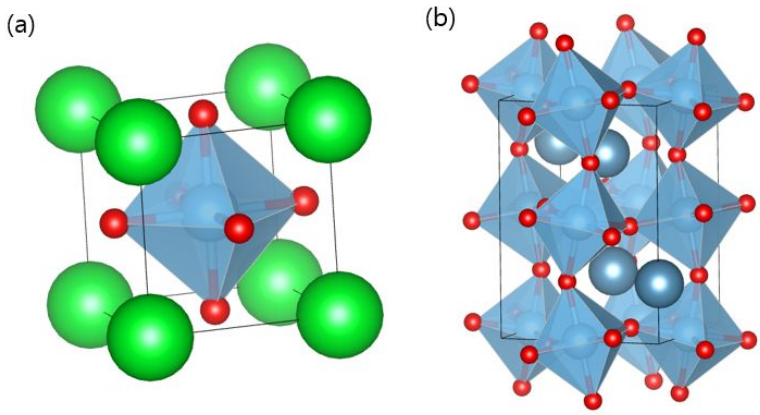

Fig 1.1 Schematic illustration of (a) cubic and (b) BO_6 octahedral tilted ABO_3 perovskite structure. Bonds between B site cation and O anion are described as polyhedrons.

1.2. Complex oxide interfaces and Two Dimensional Electron Gas (2DEG)

Transition metal oxide interfaces have gained intense interest, due to their wide range of structural, electronic and magnetic properties such as ferroelectricity, super-conductivity, magnetism, multiferroism and metal-insulator transitions. Furthermore the formation of an interface between two different oxide compounds shows new type of properties that do not exist in bulk.

A typical example of new physics emerging at oxide interfaces is found in the $LaAlO_3/SrTiO_3$ structure. [2] This system, comprised of the band insulators with large band gap ($LaAlO_3$: 5.6eV, $SrTiO_3$: 3.2eV), metallic interface is formed and completely new physics is emerged. This phenomena is called two dimensional electron gas (2DEG). The definition of 2DEG is a gas of electrons free in two dimensional sheets, but the movement is confined in the third dimension. 2DEG is first discovered in devices consist of 3-5 compound semiconductors. However, 2DEG in $LaAlO_3/SrTiO_3$ structure showed completely different behavior from that in semiconductor heterostructures.

Since the discovery of 2DEG in oxide interfaces, the origin of 2DEG is disputable. Several hypothesis are suggested, however, all of them has been unsound. In the next section, several hypotheses related to the origin of 2DEG were introduced.

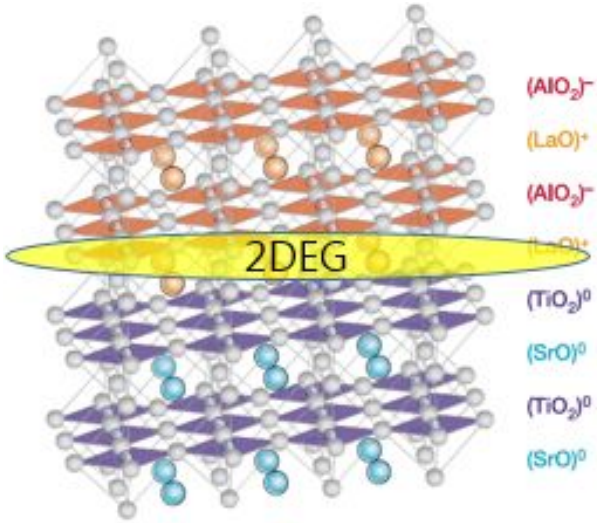

Fig 1.2 Schematic description of a 2DEG at the $LaAlO_3/SrTiO_3$ interface. 2DEG in oxide interface was firstly discovered by Othomo and Hwang [2]

1.3. Origin of 2DEG : hypotheses

1.3.1. Polarization catastrophe

The polarization catastrophe, or electronic reconstruction is initially suggested theory to explain the origin of metallic $LaAlO_3/SrTiO_3$ interface

If we look ABO_3 perovskite along [001] direction, it can be divided into two parts, AO and BO_2 planes. The cation valence of A and B can be $A^{5+}B^{1+}$, $A^{4+}B^{2+}$, $A^{3+}B^{3+}$, $A^{2+}B^{4+}$ and $A^{1+}B^{5+}$ to maintain charge neutrality. $SrTiO_3$ which has an $A^{2+}B^{4+}O_3$ has nonpolar planes whereas $LaAlO_3$ has polar planes. When film with polar planes is grown on the nonpolar planes of substrate, the electrostatic potential diverges unless any interfacial reconstruction does not occur. This phenomenon is called polarization catastrophe (See Fig 1.3). Ohtomo and Hwang suggested electronic reconstruction which shows how interface reconstruction occurs [2]. As shown in the left side of Fig 1.3, when $SrTiO_3$ is Ti-terminated, about 0.5 electrons per unit cell are injected at the interface. When electrons are injected at the interface, only Ti ions can receive electron because Ti has multi valence ions. In other words, about a half of Ti^{4+} ions at the interfacial TiO_2 planes become Ti^{3+}. On the other hand, charge injection at the interface indicates that the concentration of electrons increases. Thus, when $LaAlO_3$ is grown on $SrTiO_3$ substrate, several amount of charge carriers are concentrated at the interface, forming 2DEG.

This electron reconstruction scenario had been experimentally proved using electron energy loss spectroscopy as shown in Fig 1.4. Nakagawa et al. acquired Ti L edge EELS(Electron Energy Loss Spectroscopy) spectra, proving that several

amount of Ti^{3+} exist at the $LaAlO_3/SrTiO_3$ interface.[3] Existence of Ti^{3+} indicates high concentration of charge carriers, which is the main origin of 2DEG.

However, this scenario has some controversies. First, this theory cannot explain the metallic interface between nonpolar-nonpolar oxides. For example, $LaAlO_3$ film grown on $SrTiO_3$ (110) substrate showed metallic interface. [4] This contradicts the charge injection hypothesis. In addition, interface with conductivity was observed between amorphous $LaAlO_3$ film and $SrTiO_3$. [5]

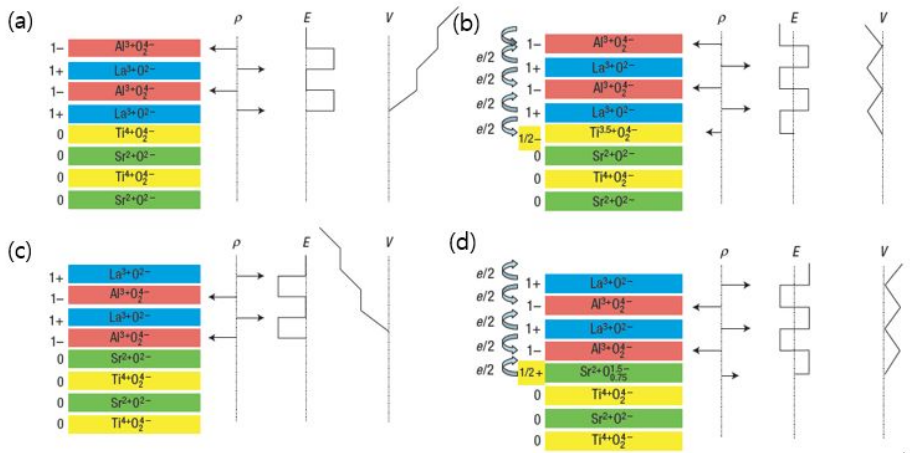

Fig 1.3 Polarization catastrophe model for atomically sharp (001) interfaces between $LaAlO_3$ and $SrTiO_3$. (a) The unreconstructed interface has neutral (001) planes in $SrTiO_3$, but the (001) planes in $LaAlO_3$ have alternating net charges (ρ). If the interface plane is $AlO_2/LaO/TiO_2$, this produces a non-negative electric field (E), leading in turn to an electric potential (V) that diverges with thickness. (b) If the interface is placed at the $AlO_2/SrO/TiO_2$ sequence instead, the potential negatively diverges. (c) The divergence of electrical potential at the $AlO_2/LaO/TiO_2$ interface can be avoided if half an electron is added to the last Ti layer. **(d)** Polarization catastrophe $AlO_2/SrO/TiO_2$ interface can also be avoided by removing half an electron from the SrO plane in the form of oxygen vacancies.

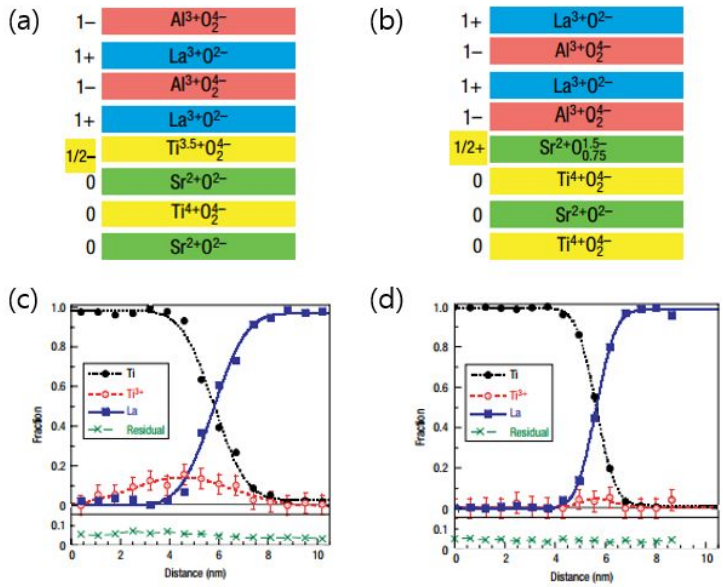

Fig 1.4 Schematic description of the electronic reconstruction at the (a) $AlO_2/LaO/TiO_2$ and (b) $AlO_2/SrO/TiO_2$ interfaces. (c) EELS intensity profile showing the fractions of Ti and La from the Ti L and La M edges at the $AlO_2/LaO/TiO_2$ interface. Ti^{3+} fraction was determined from a least-squares fit to the Ti-L edge from Ti^{3+} and Ti^{4+} reference spectra. There is excess Ti^{3+} on the substrate side of the interface (d) Corresponding Ti and La M edge profiles for the $AlO_2/SrO/TiO_2$ interface, showing almost no excess Ti^{3+}

1.3.2. Inter diffusion across the interface

The other suggested hypothesis as the origin of 2DEG is that inter diffusion between $LaAlO_3$ and $SrTiO_3$. The $LaAlO_3/SrTiO_3$ interface is far from being atomically abrupt and inter diffusion must be occur as shown by Nakagawa et al. [3] In addition, Quao et al. argued that interfaces with inter diffusion are more thermodynamically stable using first principles calculations.[5]

On the other hand, it is commonly known that several amount of charge carriers are provided to $SrTiO_3$ when La is doped to $SrTiO_3$. Even a small amount of La can increase the amount of charge carriers in $SrTiO_3$. Such a mixing can give the same effect as La doping leading to form of 2DEG in $LaAlO_3/SrTiO_3$ system. Some other physicists explain that when mixing occurs, secondary phase of $La_{1-x}Sr_xTiO_3$ is formed at the $LaAlO_3/SrTiO_3$ interface, which is close to metallic.

However, inter diffusion scenario cannot explain insulating interface of $SrTiO_3$ film on the $LaAlO_3$ substrate. This indicates that only doping effect on SrTiO3 cannot be the origin of the 2DEG. In addition, Warusawithana et al. have argued that La : Al ratio is the key factor of the formation of the 2DEG. Whether there is enough amount of inter diffusion between $LaAlO_3$ and $SrTiO_3$, 2DEG is formed only if there is excess Al in the $LaAlO_3$ films. [6] From this point of view, intermixing itself cannot explain 2DEG in $LaAlO_3/SrTiO_3$ system.

1.4.3. Role of oxygen vacancy

It is widely known that metal insulator transition occurs in $SrTiO_3$ even with a small amount of oxygen vacancy. Even if $SrTiO_3$ substrate itself is a band insulator with the gap of 3.2eV before growth, forming of oxygen vacancies during growth of $LaAlO_3$ film can lead to 2DEG in the $LaAlO_3/SrTiO_3$ system. [7]

Already in the previous work, it is confirmed that the growth conditions such as growth temperature, oxygen partial pressure greatly affect the electrical properties of the $LaAlO_3/SrTiO_3$ interfaces. In the case of low oxygen partial pressure and no annealing process before transport measurements, Ohtomo et al. found a large electron density, a high Hall mobility (10^4 $cm^2.V^{-1}.s^{-1}$) and a sheet resistance around 10^{-2} Ω/S. [2] These measurements correspond to the low oxygen partial pressure without annealing process since they are obtained by several other studies. For high oxygen partial pressure, the density reduced significantly to 10^{13}-10^{14} cm^{-2} in better agreement with the 0.5 e/u.c.[2] expected by the polarization catastrophe model. In addition, post-annealing process drops the electrical conductivity of the $LaAlO_3/SrTiO_3$ interface. [8]

In short, oxygen concentration, oxygen partial pressure during PLD growth, and the post-annealing process play an important role on the 2DEG and interfacial conductivity. However, because role of oxygen vacancy is based on the polarization catastrophe model, it is still a highly debated question.

1.4.4. Structural distortion

Some material scientists have suggested that the change of atomic structure at the interface leads to the metallic interface between insulating oxides, $LaAlO_3$ and $SrTiO_3$. On the other hand, Jang et al. reported that by inserting one atomic layer of rare-earth oxide into strontium titanium oxide, electronic properties of the interfaces can be insulator or conductor, depending on rare earth [(R is La, Pr, Nd, Sm, Y)]. [10]

Jang et al. found the origin of the difference in conductivity using STEM(Scanning Transmission Electron Microscopy)/EELS and first principles calculations. Using the fact that the transport properties of $SrTiO_3$/RO/$SrTiO_3$ interfaces are sensitive to charge carriers, ELNES (Ti L edge and O K edge) was investigated at the interfaces. As shown in Fig 1.3 (b), Ti L edge indicates that the Ti^{3+}/ Ti^{4+} ratio is almost the same at the interfaces. In addition, according to the O K edge spectra, there is a negligible amount of oxygen vacancy independent the type of the rare-earth. From this, that there are almost same amount of charge carriers are injected in all the samples can be inferred. Only charge transfer scenario cannot explain the origin of rare earth – dependent 2DEG in this system.

To understand the combined effects of charge injection, propagation of octahedral tilt, biaxial strain, and rare-earth electronic structure, Jang had carried out first principles calculations, including an on-site Coulomb interaction, or Hubbard U term. For the LaO - based heterostructure, the Fermi energy lies in the region of nonzero density of states whereas for the YO based heterostructure the Fermi energy lies between the split-off lower Hubbard band and the higher energy

density of states. This means that the LaO-based interface is conducting, whereas the YO-based interface is insulating. This is consistent with Jang's experimental results. Octahedral rotations are clearly visible in the predicted structures shown in Fig. 1.6, consistent with his synchrotron measurements.

However, those arguments are based on assumptions such as atomically abrupt interfaces. As mentioned in the previous section, atomically abrupt interface in oxide heterostructures cannot exist. Furthermore, as shown in Fig 1.3 (a), interface of $SrTiO_3$/LaO/$SrTiO_3$ does not seem to atomically abrupt. From this point of view, only strain effect and octahedral tilt cannot be the key factor of the difference of conductivities at the interfaces.

‘

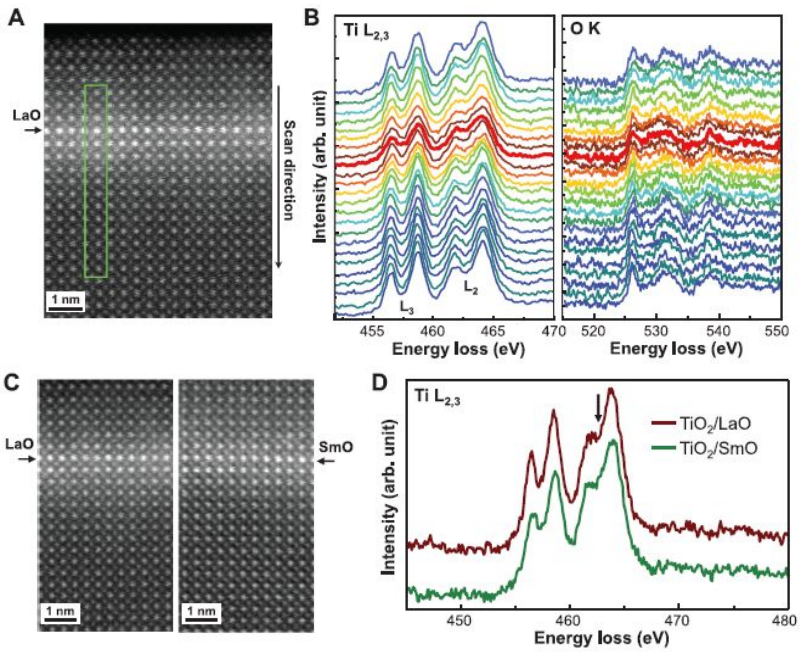

Fig 1.5. (a) Aberration – corrected High Angle Annular Dark Field (HAADF) image of a 10-uc $SrTiO_3$/1-ML LaO film grown on $SrTiO_3$. The rectangular box represents the region of EELS line scans. (b) EELS spectra of Ti-L_2, L_3 and O-K edges obtained from line scans across the interface shown in (a). The spacing along the line scan between consecutive EELS spectra is 2.8 Å. The spectra at the LaO layer are highlighted by thicker lines. For the spectra for Ti L_2 and L_3 edges, peak broadening and less pronounced peak splitting at the interface are clearly observed. (c) HAADF images of 10-uc $SrTiO_3$/1-ML LaO/$SrTiO_3$ and 10-uc $SrTiO_3$/1-ML SmO/$SrTiO_3$ heterostructures. Both samples show no obvious defects or dislocations, indicating coherent interfaces. (d) Selected area Ti-L_2, L_3 EELS spectra obtained at the interfaces for 10-uc $SrTiO_3$/1-ML LaO/$SrTiO_3$ and 10-uc $SrTiO_3$/1-ML SmO/$SrTiO_3$ heterostructures. The arrow is a guide for comparison.

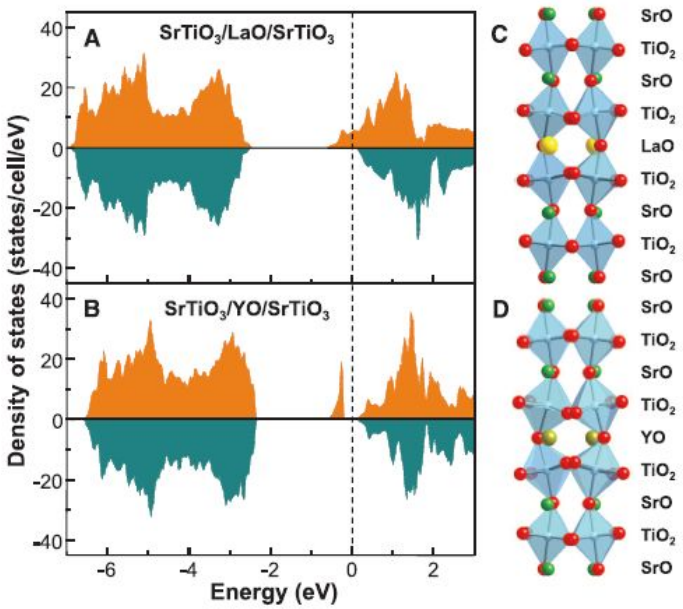

Fig 1.6 Density of states and structural relaxation of 3.5-uc $SrTiO_3$/1-ML LaO ((a) and (c) periodic superlattice and 3.5-uc $SrTiO_3$/1-ML YO periodic superlattice ((b) and (d)) obtained from DFT calculations. Positive density of states is for spin up and negative is for spin down. The dashed line indicates the position of the Fermi level. The results indicate conducting behavior for the 3.5-uc $SrTiO_3$/1-ML LaO periodic superlattice and insulating behavior for the 3.5-uc $SrTiO_3$/1-MLYO periodic superlattice.

1.4. Motivation

There is not any widely-accepted theory related to origin of 2DEG although this has been a lot of interest for more than a decade. This is because $LaAlO_3/SrTiO_3$ structure has been grown on various conditions, leading to form a wide range of atomic and electronic structure at the $LaAlO_3/SrTiO_3$ interfaces. On the other hand, in 2013, Moon et al. reported the relationship between 2DEG and interfacial composition. [11] Moon et al. insisted that interfacial conductivity can be varied from insulator to metal depend on Sr content of $Sr_xCa_{1-x}TiO_3$ films. As seen in Fig 1.6, as the Sr composition in $Sr_xCa_{1-x}TiO_3$ increased, the conductivity of the system increased by 6 orders of magnitude. This experimental data has nothing to do with electrical properties of $SrTiO_3$, $CaTiO_3$ and $Sr_{0.5}Ca_{0.5}TiO_3$ as shown in Table 1.1. Moon et al suggested that the origin of this big difference in transport properties is mainly the difference of the TiO_6 octahedral tilt angle of $SrTiO_3$, $CaTiO_3$ and $Sr_{0.5}Ca_{0.5}TiO_3$. As shown in Fig 1.5, phase contrast image was also acquired in Moon's work. In Fig 1.5 (d), (1-21) peak with a small intensity indicates that the $CaTiO_3$ film has an orthorhombic crystal structure and possesses octahedral tilting. The same result was shown in the case of the $Sr_{0.5}Ca_{0.5}TiO_3$ film.

However, only measuring octahedral tilt angle of $Sr_xCa_{1-x}TiO_3$ films cannot explain the relationship between atomic structure and 2DEG on the interfaces. Even if there is directional relationship between octahedral rotation angle and electrical properties of perovskite oxides as mentioned in the previous study [11], only differences in octahedral tilt angle cannot explain the differences in electronic structures at the interfaces. This is because first, electrical properties at the 'interface' does not have direct relationship with atomic structure of 'thin films'.

Even if non-negligible amount of octahedral rotation is observed at the $Sr_xCa_{1-x}TiO_3$ films, atomic structure of interfaces can be different from that of the perovskite films in bulk. Second, as mentioned in the previous section, atomically abrupt interfaces cannot exist. Such an intermixing at the interfaces can modify electronic states of transition metal ions, which may not mainly depend on octahedral rotations. Thus, our approach was different from what Moon et al. had suggested. [11]

Above all, there is not any report about experimental study about the electronic structures of interfaces, which directly affect the electrical properties at the $LaAlO_3/CaTiO_3$ or $LaAlO_3/SrTiO_3$ interfaces. Not only observing atomic structures of the $LaAlO_3/Sr_xCa_{1-x}TiO_3$ interfaces but also interfacial electronic structure driven by chemical or bonding states at the interfaces should be included in our research. The change of the electronic structures at the interfaces, whether they are driven by chemical reaction or strain effect can explain the origin of the difference of interfacial electrical conductivity. This is how our research is motivated.

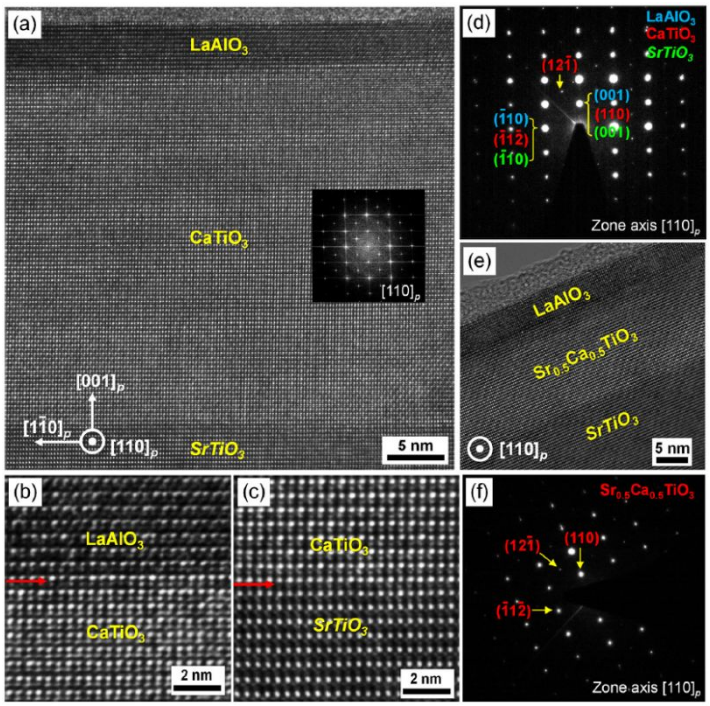

Fig 1.7 (a) HRTEM image of a $LaAlO_3/CaTiO_3/SrTiO_3$ structure. The inset is the FFT patterns from the $CaTiO_3$ layer. HRTEM images of (b) $LaAlO_3/CaTiO_3$ and (c) $CaTiO_3/SrTiO_3$ interfaces showing the sharp interface indicated by red arrows. (d) SAED pattern of the $LaAlO_3/CaTiO_3/SrTiO_3$ structure. (e) Phase contrast TEM images and (f) SAED pattern of a $LaAlO_3/Sr_{0.5}Ca_{0.5}TiO_3/SrTiO_3$ structure. (12-1) weak spot was detected in the pattern.

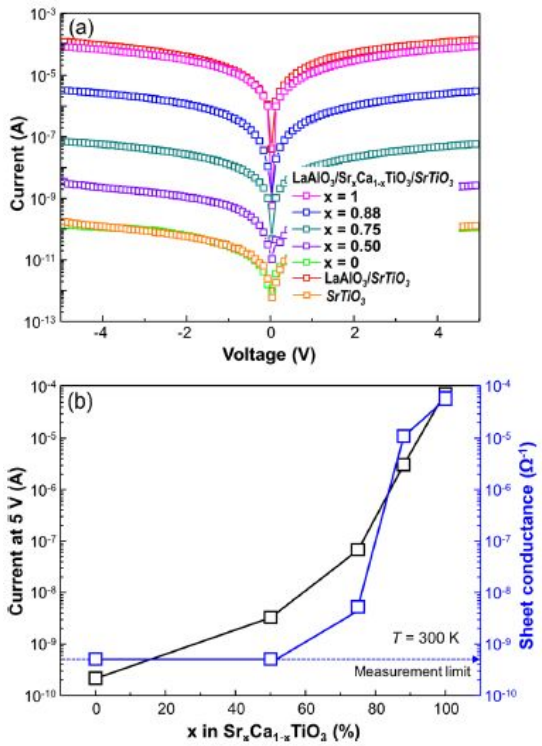

Fig 1.8 (a) Typical I-V curves of $LaAlO_3$ (5 nm)/$Sr_xCa_{1-x}TiO_3$ (10 nm)/$SrTiO_3$ structures. For comparison, I-V curves of $LaAlO_3/SrTiO_3$ and bulk $SrTiO_3$ are presented. (b) Current at 5V and sheet conductance of the $LaAlO_3/SrxCa_{1-x}TiO_3/SrTiO_3$ structures as a function of atomic composition of Sr. As the composition of Sr increased, sheet conductance increased by 6 orders of magnitude.

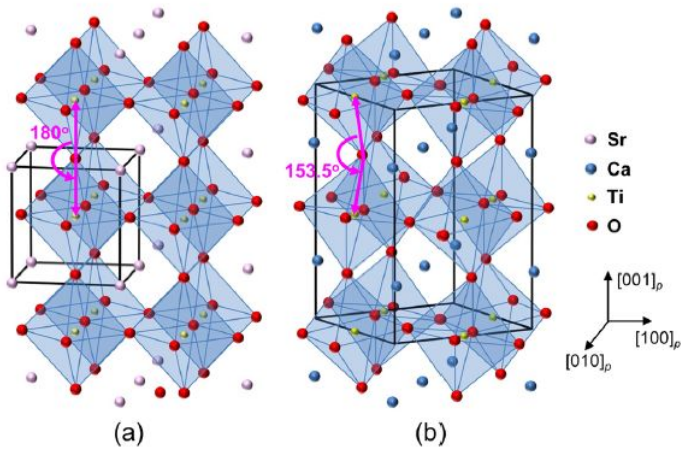

Fig 1.9 Schematic illustration of TiO_6 octahedron in cubic (a) $SrTiO_3$ and orthorhombic (b) $CaTiO_3$. Octahedral rotations in $CaTiO_3$ are highlighted by the Ti-O-Ti angle much lower than 180 degrees. This is because ionic radius of Ca is smaller than Sr, leading to lower the tolerance factor, 't'.

Compound	Conductivity at 300K $(\Omega m)^{-1}$
$CaTiO_3$	6.04×10^{-10}
$Sr_{0.5}Ca_{0.5}TiO_3$	1.68×10^{-6}
$SrTiO_3$	10^{-6}

Table 1.1 List of conductivity of $CaTiO_3$, $Sr_{0.5}Ca_{0.5}TiO_3$ and $SrTiO_3$ at the room temperature

1.5. Goal of this work

In this research, the relationship between electronic and atomic structures were inspected in the $LaAlO_3/Sr_xCa_{1-x}TiO_3/SrTiO_3$ heterostructures. (x = 0, 1.0). This research contains not only observation of atomic and electronic structures of $LaAlO_3/Sr_xCa_{1-x}TiO_3$ interfaces depending on Sr:Ca atomic ratio, but also investigation of the relationships between them. Our main question on this research is 'How inter diffusion between $LaAlO_3$ and $Sr_xCa_{1-x}TiO_3$ affect interfacial conductivity?' and 'Can octahedral tilt in $Sr_xCa_{1-x}TiO_3$ affect electrical property of interfaces? Our research is divided into two parts.

First, this work is proposed to compare electronic structure of the interfaces between $LaAlO_3$ and $Sr_xCa_{1-x}TiO_3$ films. Using core-loss EELS (ELNES), the differences in Ti L edge and O K edge were observed. Interpretation of the EELS spectra can determine whether the new chemical states are formed at the $LaAlO_3/Sr_xCa_{1-x}TiO_3$ interfaces.

The second part of this thesis is focused on direct observation of the atomic structures of the $LaAlO_3/Sr_xCa_{1-x}TiO_3$ interfaces. Using Cs corrected STEM, we directly observed the atomic structure of the interfaces. Of course, roughness of the oxide interfaces are strongly dependent on the growth conditions. However, the existence of interfacial bonding state is independent of growth condition considering the noticeable difference in electronic properties of interlayer $Sr_xCa_{1-x}TiO_3$ films.

The research is not focused on interface itself but the relationship between

atomic structures and electronic structures at the $LaAlO_3/Sr_xCa_{1-x}TiO_3$ interfaces.

Chapter 2. Experimental Method

2.1 TEM sample preparation

TEM analysis requires an enough thin specimen that electron beam can transmit through it. When the specimen is not thin enough, multiple scattering events can occur, leading to artifacts in the diffraction and inelastic scattering information. Electron transparent specimen can be accomplished by mechanical polishing and Ar ion milling. This procedure is depicted for a cross sectional TEM sample of an epitaxial film in Fig. 3.1. A $SrTiO_3$ substrate with the same film is glued to the surface of the film using M Bond 610 and placed on a hot plate at 195°C for at least 3 hours. The sandwich is then sectioned into 1.5mm slices by a diamond cutting saw. The cross section surface is then mounted with crystal wax to a multiprep polisher pyrex holder and polished using a series of progressively finer diamond lapping film under water flow (9, 6, 3, 1μm), usually ending with 0.5μm with the lubricant. The sample is then flipped, remounted, and polished until the overall specimen thickness becomes less than 10 μm. The specimen is then soaked in acetone until the sample falls free. A molybdenum slot grid is then glued to the 2nd polished surface and allowed to dry for at least 3-4 hours under the IR lamp. The specimen with Mo slot grid is Argon ion milled in a Gatan precision ion polishing system (PIPS). The sample is ion milled from both the top and bottom surfaces with the ion beam oriented normal to the interface. The angle and energy of the ion guns is progressively reduced from an initial setting of ±6° and 3.5 keV ultimately to a ±5° and 500 eV surface cleaning step. To minimize the heating effect and surface damage on the specimen, liquid nitrogen was poured into the

PIPS system. The paired $SrTiO_3$ is milled preferentially and the process is stopped when the $SrTiO_3$ just barely covers the film. The finished sample usually appears as in Fig. 2.1

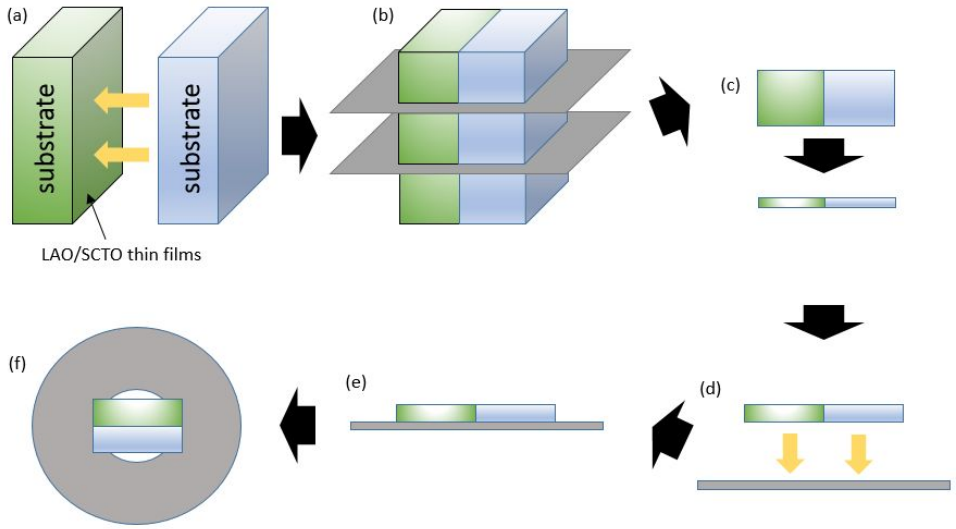

Fig 2.1 Schematic diagram of the TEM sample preparation using polishing and precision ion milling (a) Thin film specimen is glued to another. (b) After curing, the whole specimen was sectioned. (c) Sectioned specimen is polished until its thickness gets under 10μm. (d) After the thinned specimen is separated from the pyrex holder, it is glued to molybdenum slot grid. (f) Top view of the specimen with the Mo grid. Finally, the specimen was thinned using PIPS system.

2.2 Film characterization

2.2.1. Sheet resistance measurement

As performed in the previous work, sheet resistance of the heterostructures was measured using indium ohmic contacts on the diagonal corners of the square samples

2.2.2. Atomic Force Microscopy (AFM)

After conductivity of the heterostructures was measured, AFM images were acquired. From AFM image, we could confirm the surface profile of the thin films.

2.3 TEM characterization

To investigate the relationship between atomic, electronic structure and electrical properties of the interfaces, several modes of TEM will be used. Especially, advanced analytical technique such as Cs corrected HAADF STEM and EELS will be taken advantage of.

2.3.1 HRTEM imaging

Using phase contrast high resolution imaging, crystal structure of $Sr_xCa_{1-x}TiO_3$ films were investigated. Then, uniformity of the $Sr_xCa_{1-x}TiO_3$ on the $SrTiO_3$ substrate can be confirmed. HRTEM images were obtained with a 200-kV field-emission TEM instrument (JEOL JEM-2100F).

2.3.2 Cs – corrected HAADF / ABF STEM imaging

To investigate atomic structure of the interfaces, Cs-corrected high resolution STEM images were obtained with Cs-probe corrected TEM instrument (JEOL JEM ARM 200F). STEM imaging with spherical aberration (Cs) corrector provides more clear images with spatial resolution of 80pm. Thus Cs corrected HR-STEM imaging enables not only identifying elements but also finding atomic positions in high accuracy.

Images are obtained in HAADF and ABF STEM modes simultaneously. Especially, in this research, aberration – corrected high resolution STEM images were obtained.

In HAADF STEM mode, scattered electrons in high angle (Fig 2.1) is collected to the detector, leading to formation of the images. Because detected electrons in high angle are Rutherford-scattered, intensity of the HAADF STEM image is approximately proportional to the square of the atomic number. In this sense, HAADF STEM imaging is beneficial to observe heavy elements such La, Pr, Sm, Ir but this mode cannot find the position of light elements such as Li, Be, N, O.

On the other hand, ABF imaging is advantageous to identify the light elements. In our work, using ABF imaging technique, B-O-B bonding angle can be measured in ABO_3 perovskite oxides.

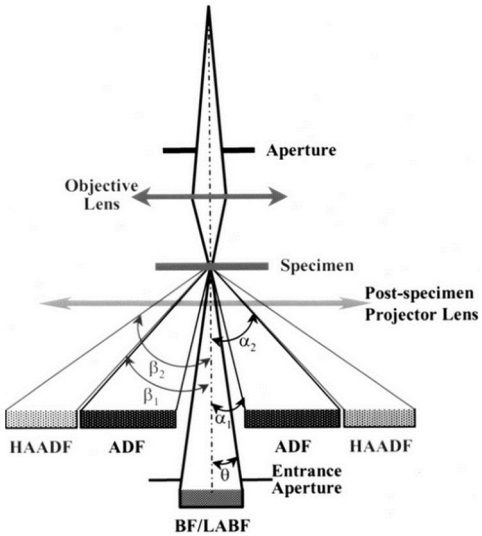

Fig 2.2 Schematic illustration of STEM. Depending on the electron scattering angle, HAADF, ADF, BF and LAADF STEM image can be obtained. [12]

2.3.3 EELS

When a specimen in TEM has an interaction with a beam of electrons, elastic / inelastic scattering of electrons occur. In case of elastic scattering, kinetic energy of the electrons are preserved whereas electrons loss their energy and kinetic paths are randomly modified when electrons are under inelastic scattering. The amount and the electron distribution of energy loss can be measured via a spectrometer. Analyzing this data is called EELS. Inelastic scattering of electrons come in various forms such as plasmon and phonon excitations, transition of energy states, inner shell ionizations.

EELS can be taken advantage of various quantitative analysis such as thickness measurement of the specimen, stoichiometric analysis, valence measurement of transition metal ions, etc. EELS can be divided two parts, low loss spectra and core-loss spectra. Core loss spectra reflects transition states of electrons in the specimen when electrons are interacted with it. In our work, Ti L edge and O K edge spectrums were acquired. In particular, Ti L edge spectra contains information of valence of Ti cations. As shown in Fig 2.1, EELS spectrum of Ti^{3+} and Ti^{4+} are definitely different. Using this as reference, the valence state of Ti at the interfaces were investigated.

On the other hand, O K edge at the interfaces were also investigated. By analyzing O K edge, we can qualitative determine the amount of oxygen vacancy and the bonding state at the interfaces.

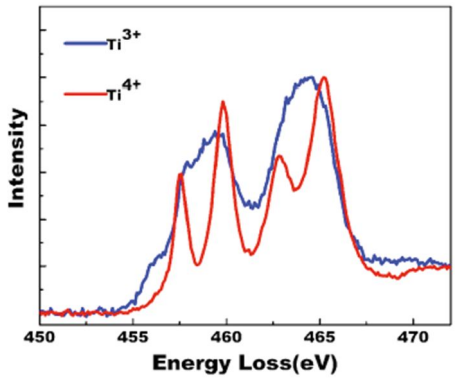

Fig 2.3 Core loss spectra acquired from the reference sample Ti^{3+} from LaTiO3 and Ti^{4+} from $SrTiO_3$ with the same specimen thickness and same experimental conditions. [10]

Chapter 3. Results and Discussions

3.1 Reproducibility of the $LaAlO_3/Sr_xCa_{1-x}TiO_3/SrTiO_3$ system

3.1.1 Conductivity measurement

To check the reproducibility of the $LaAlO_3/Sr_xCa_{1-x}TiO_3/SrTiO_3$ system, we measured the electrical resistance using the same method as performed in the previous work. We also compared our data with what Moon had measured. As shown in Table 3.1, there is a difference in the resistivity by 1~2 orders of magnitude. However, in case of $LaAlO_3/CaTiO_3/SrTiO_3$, sheet resistance could not be measured because the value is over the limit of the resistance-measuring device so we could not measure the electrical property of this structure in precise. Still, as already shown in Moon's work, metal insulator transition depending on composition of Sr has been confirmed. The difference between our experiment and previous work would be discussed in the section 3.1.4.

structure	experiment	reference
$LaAlO_3/CaTiO_3/SrTiO_3$	Over tolerance	10^{10}
$LaAlO_3/SrTiO_3$	8×10^5	10^4

Table 3.1. Sheet resistance of $LaAlO_3/CaTiO_3/SrTiO_3$ and $LaAlO_3/SrTiO_3$ structure (units : Ω). Comparison with the reference [9] is included.

3.1.2 AFM image

Fig 3.1 corresponds to surface profile image of the $LaAlO_3/CaTiO_3/SrTiO_3$ and $LaAlO_3/SrTiO_3$ system. In Fig 3.1 (a), step and terrace profile was observed. This indicates that $CaTiO_3$ and $LaAlO_3$ film were deposited in high quality without several amount of misfit dislocations.

On the other hand, in Fig 3.1 (b), step and terrace pattern was not clearly observed. However, considering that measured roughness is less than 1nm, we concluded that 1~2 unit cells of roughness exists on the $LaAlO_3$ surface. This result is not seem to be directly related to crystalline quality of the samples.

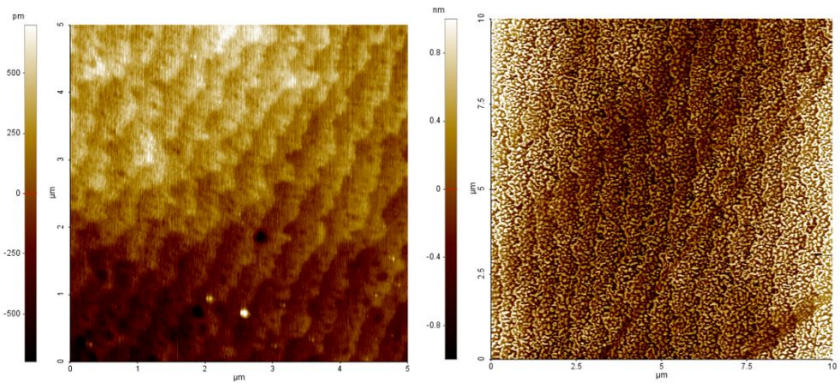

Fig 3.1. AFM images of a (a) $LaAlO_3/CaTiO_3/SrTiO_3$ and (b) $LaAlO_3/SrTiO_3$ structures.

3.1.4 HRTEM (Phase contrast) imaging

Although quality of thin films are verified using characterization tools such as XRD and AFM, these techniques cannot identify dislocations, point defects, grain boundaries in the films and interfaces between films and $SrTiO_3$ substrates. However, HRTEM imaging enables us identify point and planar defects in the oxide heterostructures and give feedbacks on optimizing growth condition of thin films. In addition, the quality of TEM specimens were identified.

3.1.4.1 $LaAlO_3/CaTiO_3/SrTiO_3$

Fig 3.2 refers to a cross-sectional HRTEM image of a $LaAlO_3/CaTiO_3/SrTiO_3$ structure. It is evident that $CaTiO_3$ film is poly crystal and grain boundaries are distributed in the periodic arrangement. This indicates that the strain was relaxed when the $CaTiO_3$ film was deposited on $SrTiO_3$ substrate. However, the stripe pattern is observed in the Region 2. Even if $CaTiO_3$ has an orthorhombic crystal symmetry, experimental image of the film is similar to that of $SrTiO_3$ substrate. To demonstrate this, we performed HRTEM simulation using JEMS program. As shown in Fig 3.4, HR image of stoichiometric $CaTiO_3$ film does not have a stripe pattern. This indicates that in the Region 2, ion vacancy is ordered like brownmillerite phase. We additionally investigated grain distribution of $CaTiO_3$ film to grasp how $CaTiO_3$ film was deposited. The result is shown in Table 3.2. Each grain was almost uniformly formed in the $CaTiO_3$ film.

It is generally accepted that defects such as grain boundaries, dislocations in the films can be the source of higher resistivity of the complex oxide heterostructures

compared to oxide system without any defects. Thus, observed defects in the $CaTiO_3$ film can be the cause of increased sheet resistance compared to that of the previous report. [9]

3.1.4.2 $LaAlO_3/SrTiO_3$

Growth of $SrTiO_3$ film on $SrTiO_3$ substrate had not been on optimized condition so our work could not follow the previous work in precise. Instead, $LaAlO_3$ film was directly deposited on $SrTiO_3$ substrate. As shown in Fig 3.2 (d), $LaAlO_3$ film was grown with high crystalline quality. In addition, there is no misfit dislocations in the $LaAlO_3$ film and $LaAlO_3/SrTiO_3$ interface seemed to be sharp. We could not find the cause of the difference in the sheet conductance compared to the previous work. [9]

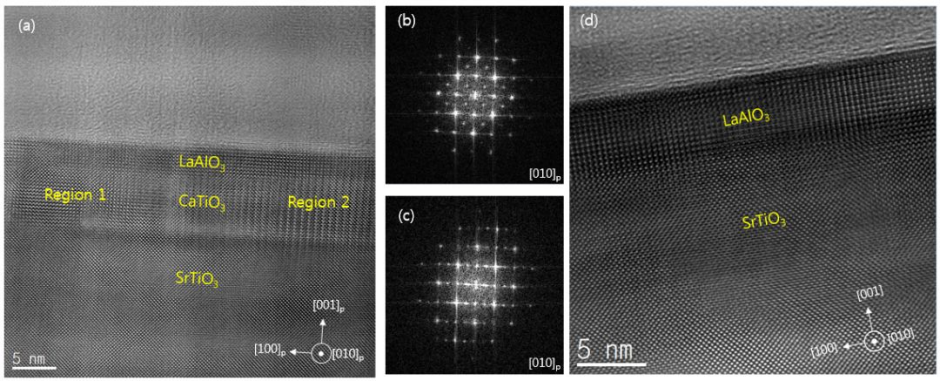

Fig 3.2 (a) ABSF – filtered Cross-sectional HRTEM image of the $LaAlO_3/CaTiO_3/SrTiO_3$ structure on the $[010]_p$ zone axis. $CaTiO_3$ film was grown in polycrystalline. (b) FFT diffraction patterns from the Region 1 of the $CaTiO_3$ layer. (c) FFT diffraction patterns from the Region 2 of the $CaTiO_3$ layer. (d) ABSF – filtered Cross-sectional HRTEM image of the $LaAlO_3/SrTiO_3$ structure on the $[010]_p$ zone axis. $LaAlO_3$ film was epitaxially grown on the $SrTiO_3$ substrate. The $LaAlO_3/SrTiO_3$ interface looks sharp.

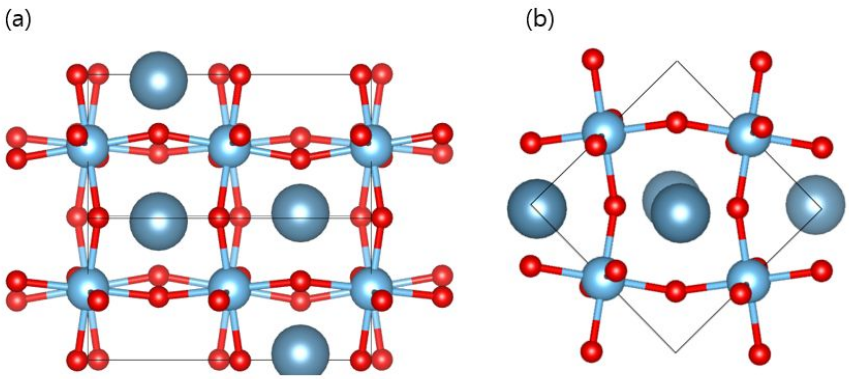

Fig 3.3 Projection of $CaTiO_3$ atomic unit cell on the (a) $[100]_p$ and (b) $[001]_p$ zone axis using ball and stick model. In the case of (a), out of phase octahedral tilt can be observed whereas in phase octahedral tilt is observed in the case of (b). This is because the Glazer notation of $CaTiO_3$ is $a^- a^- c^+$.

Zone axis	counts	Average (nm)
$[100]_p$	5	22.000±4.777
$[001]_p$	8	15.833±4.238
$[100]_p + [001]_p$	10	13.671±1.764

Table 3.2 Distribution, size of the two type of grains in the polycrystalline $CaTiO_3$ film.

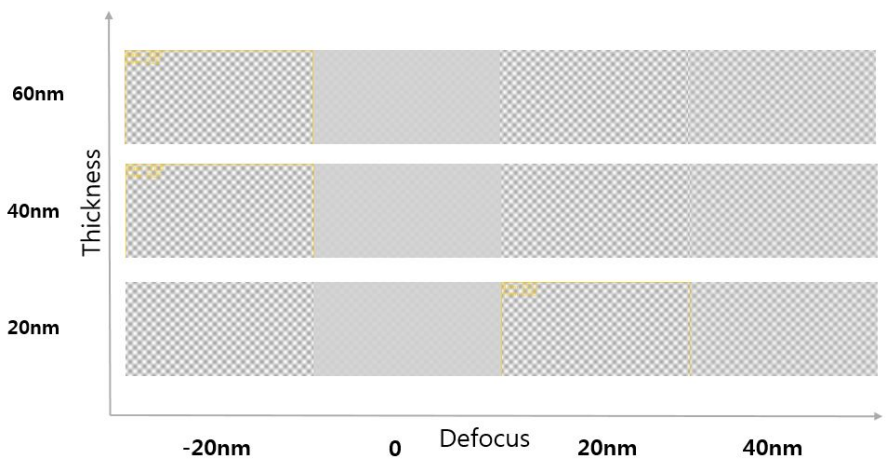

Fig 3.4 Simulated HR image of stoichiometric $CaTiO_3$ on the $[100]_p$ zone axis. Stripe pattern is not observed in the simulated image.

3.2 Atomic-scale observation of the $LaAlO_3/Sr_xCa_{1-x}TiO_3/SrTiO_3$ interfaces

After the quality of $LaAlO_3/Sr_xCa_{1-x}TiO_3/SrTiO_3$ structures and TEM specimens were confirmed, atomic structure of the $LaAlO_3/Sr_xCa_{1-x}TiO_3$ interfaces were investigated. Using spherical aberration – corrected high resolution STEM imaging, atomic structure of the interfaces were identified. Particularly, ABF STEM imaging enabled us to measure bonding angle between Ti, O, and Ti atomic columns at the interfaces. To measure octahedral tilt angle in precise, Peak Pairs Analysis (PPA) method was used in this work.

3.2.1 HADDF STEM

3.2.1.1 $LaAlO_3/CaTiO_3/SrTiO_3$

Fig 3.4 refers to the HAADF STEM image of the $LaAlO_3/CaTiO_3/SrTiO_3$ structure. Each atomic column of the component is marked as circles. The image shows that the interface is atomically sharp without any inter diffusion across the interfaces. We also analyzed the $CaTiO_3$ part of the HAADF STEM image. As shown in the Fig 3.6, the observed $CaTiO_3$ part is correspond to the $CaTiO_3$ [100]p projection. Because TiO_6 octahedrons were rotated out of phase, when ABF STEM image is acquired in the same region, oxygen atomic columns would be averaged out so octahedral tilt angle is cannot be observed.

3.2.1.2 $LaAlO_3/SrTiO_3$

Fig 3.5 refers to the Z-contrast STEM image of the $LaAlO_3/SrTiO_3$ structure. The image indicates that the interface is atomically sharp. However, as shown in Fig 3.4

(b), the intensity of the A site does not changes abruptly, which indicates there is several amount of inter diffusion (in about 4 unit cells)

However, HAADF STEM imaging can hardly detect the position of O columns so we could not measure octahedral tilt angle in the HAADF mode. Then, ABF STEM imaging technique was used. ABF STEM images were simultaneously acquired.

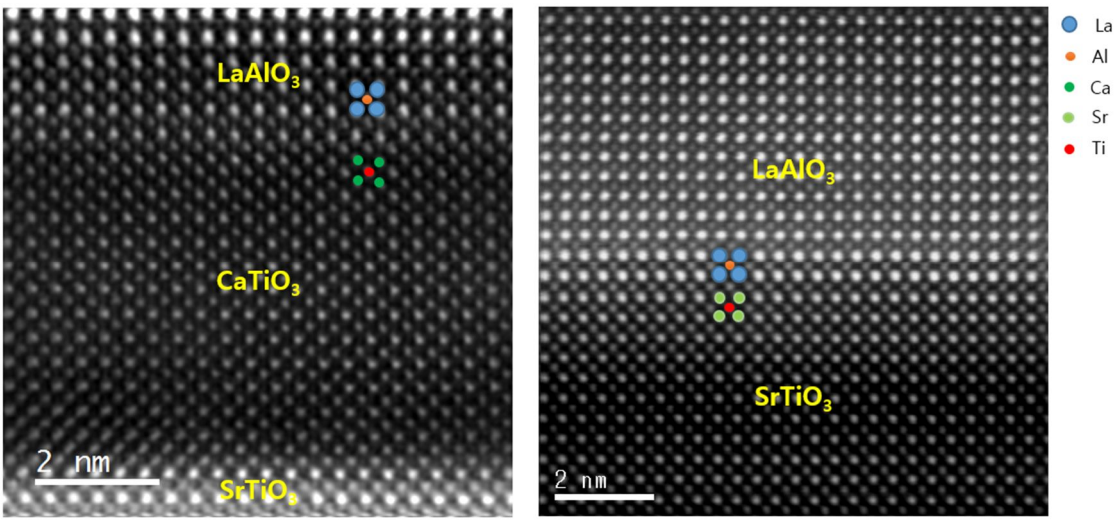

Fig 3.5 Cs corrected high resolution HAADF STEM image of (a) $LaAlO_3/CaTiO_3/SrTiO_3$ and (b) $LaAlO_3/SrTiO_3$ structures. Interfaces are atomically sharp in both.

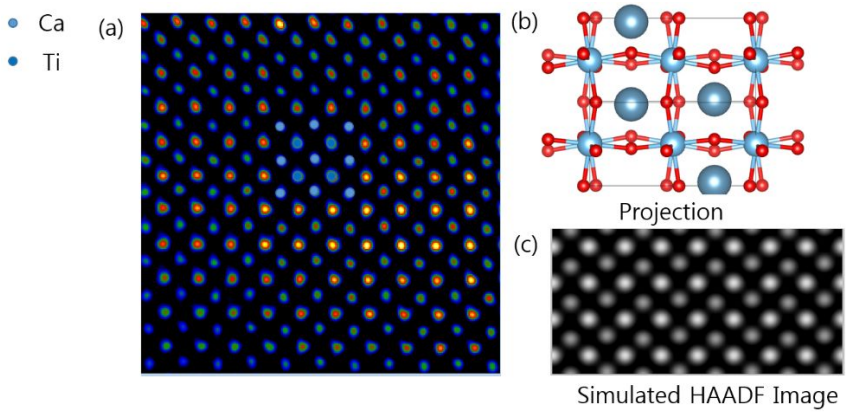

Fig 3.6 (a) HAADF STEM image of the $CaTiO_3$ film. (b) $[100]_p$ projection of the CaTiO3 film. Image (a) is observed in this projection. (c) Simulated HAADF image of the $CaTiO_3$ film. This well matches with the experimental image.

3.2.2 ABF STEM imaging

3.2.2.1. $LaAlO_3/CaTiO_3/SrTiO_3$

As shown in Fig 3.3, even if several amount of octahedral rotation exists, we should observe $CaTiO_3$ film on particular zone axis. If $CaTiO_3$ image is obtained on the $[100]_p$ or $[010]_p$ zone axis, oxygen atomic columns would be averaged out. This is because on the $[100]_p$ and $[010]_p$ zone axis, TiO_6 octahedrons are rotated out of phase. Oxygen signals are averaged out so the amount of octahedral rotation cannot be measured. Instead, we found the region where the projection of $CaTiO_3$ on the $[001]_p$ zone axis is observed and then, ABF image was acquired. To measure Ti-O-Ti bonding angle in precise, we conducted peak pairs analysis to find atomic position of Ti and O.

As shown in Fig 3.5, considerable amount of octahedral rotation was observed in the $CaTiO_3$ film far from the $LaAlO_3/CaTiO_3$ interface. Due to the tensile strain on the $CaTiO_3$ film, the TiO_6 octahedral tilt angle was increased compared to bulk. To analyze it quantitatively, we measured Ti-O-Ti angle position by position. We averaged all the angles in the same line of the position as denoted in the Fig 3.6 (b) which indicates that the octahedral tilt angle of $CaTiO_3$ near the interface is larger than that of $CaTiO_3$ far from the interface. Because the $CaTiO_3$ film is biaxially tensile strained, the whole Ti-O-Ti bond angle is smaller than that of bulk.

3.2.2.2 $LaAlO_3/SrTiO_3$

Fig 3.5 (b) refers to the high resolution ABF STEM image of the $LaAlO_3/SrTiO_3$ structure. As shown in the Fig, there is a negligible TiO_6 octahedral tilt at the $LaAlO_3/SrTiO_3$ interface. The result of PPA also showed the same as directly shown in the image. This result is self-consistent considering that the Ti-O-Ti bonding angle is exactly 180 degrees even if the $SrTiO_3$ substrate near the interface is compressively strained.

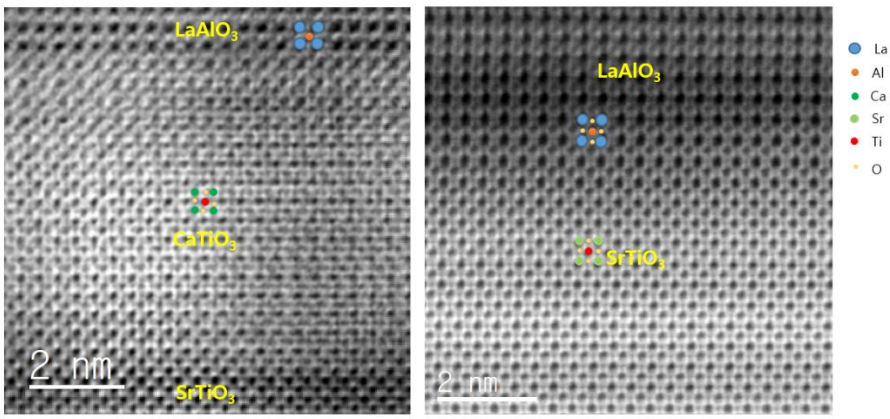

Fig 3.7 Aberration corrected high resolution ABF STEM image of (a) $LaAlO_3/CaTiO_3/SrTiO_3$ and (b) $LaAlO_3/SrTiO_3$ structures. Octahedral tilt has been observed in the $CaTiO_3$ film whereas there is not any octahedral rotation in the $SrTiO_3$ substrate in the $LaAlO_3/SrTiO_3$ structure. Each atomic columns are marked as colored circles.

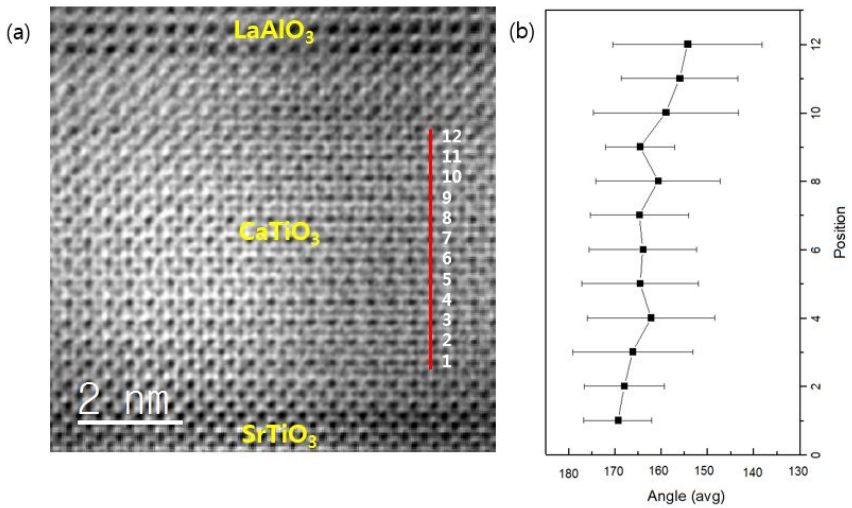

Fig 3.8 (a) High Resolution ABF STEM image of the $LaAlO_3/CaTiO_3/SrTiO_3$ structure. Ti-O-Ti angle had been measured by averaging all of the angles in the same line. The number of the lines are denoted in the image. (b) Average angle distribution of the $CaTiO_3$ film. Error bars are correspond to standard deviation.

3.3 Investigation of the electronic structures at the interfaces (EELS)

After observing the atomic arrangement of the interfaces, electronic structures were obtained using monochromated EELS. EELS spectra were obtained from FEI Titan 80-300.

3.3.1. $LaAlO_3/CaTiO_3/SrTiO_3$

To identify the change in chemical states at the interface, we first acquired Ti L edge spectra from the $CaTiO_3$ film and the $LaAlO_3/CaTiO_3$ interface.

There is not a significant change in Ti L edge at the $LaAlO_3/CaTiO_3$ interface as shown in Fig 3.9. We also measured the peak position of L_3, L_2 edge and calculated L_3/L_2 ratio in the case of the $SrTiO_3$ substrate and the $LaAlO_3/SrTiO_3$ interface. The white line ratio (L_3/L_2 ratio) is hardly decreased from the $CaTiO_3$ film to the $LaAlO_3/CaTiO_3$ interface (See Table 3.4). However, we can see that Ti^{3+} was observed in the whole $CaTiO_3$ film. The ratio of Ti^{3+} is roughly confirmed by comparing Ti L edge of $CaTiO_3$ with that in the $SrTiO_3$ substrate in the $LaAlO_3/SrTiO_3$ system. This is due to non-stoichiometric growth of $CaTiO_3$, which leads to valence shift of Ti ions to compensate ordered defects.

The Ti L edge spectra at the interface in this work is similar to what the previous work have expected. Although considerable amount of Ti^{3+} is detected at the $LaAlO_3/CaTiO_3$ interface and $CaTiO_3$ is not grown in the stoichiometric condition, the interface is still an insulator. In this sense, regardless of the amount of Ti^{3+} at the interface, octahedral rotation plays a crucial role determining interfacial

conductivity.

3.3.2. $LaAlO_3/SrTiO_3$

Compared to Ti L edge spectra in the $SrTiO_3$ substrate, there is a significant change in Ti L edge at the $LaAlO_3/SrTiO_3$ interface as shown in Fig 3.9. There is less orbital splitting of Ti L edge at the interface. [11] This result is contrast to the case of $LaAlO_3/CaTiO_3$ where no significant change in Ti L edge spectra is observed. We also calculated L_3/L_2 ratio in the case of the $SrTiO_3$ substrate and the $LaAlO_3/SrTiO_3$ interface. As expected, the white line ratio (L_3/L_2 ratio) is considerably decreased from $SrTiO_3$ substrate to the $LaAlO_3/SrTiO_3$ interface (See Table 3.2).

The significant change in Ti L edge at the interface can be interpreted as the transition in the valence of Ti ions. [10] Comparing with Ti L edge from $SrTiO_3$ (Ti^{4+}) and Ti L edge from $LaTiO_3$ as shown in Fig 2.3, we can argue that substantial proportion of Ti ions were under the reduction. Or, Ti L edge spectra at the interface can be considered as the linear combination of EELS spectra of Ti^{4+} (from $SrTiO_3$) and Ti^{3+} (from $LaTiO_3$). Already, in the previous studies, change of Ti valence at the $LaAlO_3/SrTiO_3$ interfaces had been detected. Most of the previous work interpreted this change(s) as the way of avoiding polarization catastrophe, called interfacial electronic reconstruction.

On the other hand, there is not a significant change in O K edge from $SrTiO_3$ substrate to the interface. There is a negligible amount of oxygen vacancy at the interface. This indicates that Ti^{3+} at the interface is not come from oxygen vacancies. Instead, shift of valence state if Ti ion is due to the formation of

interfacial chemical states.

However, as mentioned in the previous section, there is not significant change in Ti ion valence at the interface in the case of the $LaAlO_3/CaTiO_3/SrTiO_3$ system but because $CaTiO_3$ is grown on nonstoichiometric condition, nearly half portion of Ti^{3+} ions were detected. However, considering conductivity measurement data, the emergence of Ti^{3+} does not directly affect the formation of 2DEG.

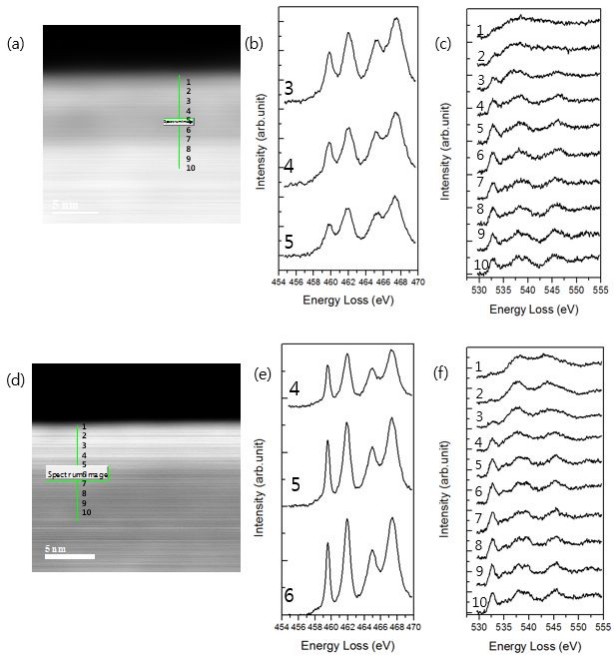

Fig 3.9 (a) HAADF STEM image, (b) Ti L edge and (c) O K edge of the $LaAlO_3/CaTiO_3/SrTiO_3$ structure. (d) HAADF STEM image,(e) Ti L edge and (f) O K edge of the $LaAlO_3/SrTiO_3$ structure.

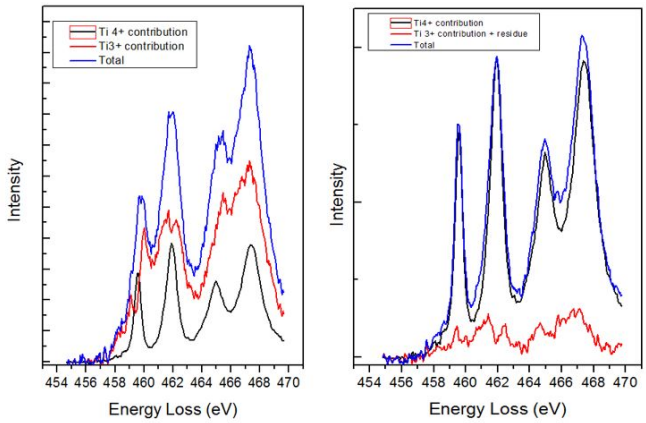

Fig 3.10. Ti L edge at the (a) $LaAlO_3/CaTiO_3$ and (b) $LaAlO_3/SrTiO_3$ interface. Both interfaces contain Ti^{3+} ions. Ratio of Ti^{3+} at the $LaAlO_3/CaTiO_3$ interface is higher than that of $LaAlO_3/SrTiO_3$ interface because $CaTiO_3$ is grown in non-stoichiometric condition. Ti^{3+} was observed not only at the interface but whole the $CaTiO_3$ film.

Position	L_3/L_2 ratio ($LaAlO_3/CaTiO_3$)	L_3/L_2 ratio ($LaAlO_3/SrTiO_3$)
1	**X**	**X**
2	**X**	**X**
3	**0.79**	**X**
4	**0.79**	**0.93**
5	**0.82**	**0.94**
6	**0.81**	**0.99**
7	**0.81**	**0.99**
8	**0.86**	**1.00**
9	**0.91**	**0.98**
10	**0.87**	**1.01**

Table 3.3 Peak position of L_2, L_3 (in eV) and L_3/L_2 intensity ratio in the $LaAlO_3/CaTiO_3/SrTiO_3$ and $LaAlO_3/SrTiO_3$ structure. Each positions are marked in the HAADF STEM image as shown in Fig 3.9.

Chapter 4. Summary and Conclusions

In this work, atomic, electronic structures and bonding states at the $LaAlO_3/CaTiO_3$ and $LaAlO_3/SrTiO_3$ interfaces and the relationship between them were investigated. In the previous work, microscopic studies related to 2DEG is focused on the $LaAlO_3/SrTiO_3$ interfaces but there is no established theory to explain 2DEG in the $LaAlO_3/SrTiO_3$ structure. Recently, there were attempts to discover 2DEG in the other oxide interfaces but the origin of 2DEG in the other system has not been studied using TEM and EELS.

Using Cs corrected STEM and monochromated EELS, we studied $LaAlO_3/CaTiO_3/SrTiO_3$ and $LaAlO_3/SrTiO_3$ system. This research is in an extension of Moon's work. This is the first trial to compare electronic structures of the $LaAlO_3/CaTiO_3$ and $LaAlO_3/SrTiO_3$ interfaces using EELS. Our experiment showed the same tendency in electrical property as Moon has already reported. [7] However, in the case of the $LaAlO_3/CaTiO_3/SrTiO_3$ structure, the deviation from the previous work is come from periodic arrangement of grain boundaries in the $CaTiO_3$ film.

Using HAADF and ABF STEM imaging, we directly observed the interfacial atomic structure. Both $LaAlO_3/CaTiO_3$ and $LaAlO_3/SrTiO_3$ interfaces are relatively atomically abrupt. In addition, as expected, considerable amount of octahedral tilt was observed in the $CaTiO_3$ film whereas Ti-O-Ti angle is near 180 degrees at the $LaAlO_3/SrTiO_3$ interface.

Using EELS, we identified the electronic structure of the interfaces. In particular,

we compared Ti L edge spectra in the $LaAlO_3/CaTiO_3/SrTiO_3$ and $LaAlO_3/SrTiO_3$ system. Unlike Jang's work, there is a significant difference in the Ti L edge spectra between in the case of the $LaAlO_3/CaTiO_3$ and $LaAlO_3/SrTiO_3$ interface. We can conclude that regardless of the stoichiometry of the $CaTiO_3$ films and-amount of Ti^{3+} ions at the interface, TiO_6 octahedral tilt plays a crucial role determining interfacial conductivity. However, in our research, $LaAlO_3/Sr_{0.5}Ca_{0.5}TiO_3/SrTiO_3$ structure has not been investigated. This will be studied in the future work.

Chapter 5. References

1. M. Imada et al. Rev. Mod. Phys. 70, 1039 (1998)
2. Ohtomo et al. Nature 427, 423 (2004)
3. N. Nakagawa et al. Nat mater. 5, 204 (2006)
4. G. Herranz et al. Sci. Rep. 2, 758 (2012)
5. Y. Chen et al. Nano Letters 11, 9 (2011)
6. M. P. Warusawithana et al. Nat Commun. 4, 2351 (2013)
7. Z. Q. Liu et al. Phys. Rev. X 3, 021010 (2013)
8. G. Herranz et al. Phys. Rev. Lett 98, 216803 (2007)
9. A. Kalabukhov et al. Phys. Rev. B 75, 121404(R) (2007)
10. H. W. Jang et al. Science 331, 886 (2011)
11. S. Y. Moon et al. Appl. Phys. Lett. 102, 012903 (2013)
12. David B. Williams et al, Transmission Electron Microscopy A Textbook for Materials Science 2nd edition (2009)
13. J. Lee et al. Appl. Phys. Lett. 106, 071601 (2015)

초 록

산화물 이차원 전자 가스는 2004년에 $LaAlO_3/SrTiO_3$ 계면에서 발견된 이래로 지금까지 연구의 관심 대상이 되어 왔다. 발견된 이례로 지금까지 근원을 밝혀내기 위한 연구들이 진행되어있지만 정립된 이론은 전무한 상황이다. 한편 2013년에는 $LaAlO_3/Sr_xCa_{1-x}TiO_3/SrTiO_3$ 의 복합구조 계면의 전기적 특성에 대하여 연구한 논문이 발표되었다. 이 논문에서는 x의 값이 증가할수록 계면의 전도도가 여섯 오더 정도 증가하는 것을 확인하였는데, 그 이유를 $Sr_xCa_{1-x}TiO_3$ 내에 존재하는 TiO_6 팔면체 틀어짐 각도의 차이에서 기인한다고 제안하였다.

본 연구에서는 각 페로브스카이트 결정구조를 지니는 $LaAlO_3/CaTiO_3/SrTiO_3$ 및 $LaAlO_3/SrTiO_3$ 산화물 복합구조의 원자 및 전자 구조를 구면 수차보정 투과전자현미경 및 전자에너지 손실 분광을 이용하여 관찰하였다. 펄스 레이저 증착 기법을 이용하여 두 시스템을 증착한 결과 이전에 연구된 바와 같이 전도도의 경향성이 동일하게 관찰되었다. 고분해능 주사투과전자현미경 이미지를 이용하여 두 구조를 관찰하였을 때 $CaTiO_3$ 박막에는 TiO_6 팔면체 틀어짐이 상당히 존재하는 반면, $LaAlO_3/SrTiO_3$ 에서 $SrTiO_3$ 기판에는 무시할 수 있을 정도로 존재하지 않는 모습을 보였다. 한편, 두 시편의 전자구조를 관찰한 결과 두 시편에서 모두 Ti 3가 양이온이 발견되었다. 이로부터 계면에서의 Ti 3가 이온의 비율에 관계 없이 팔면체 틀어짐이 계면의 전기적 성질을 결정하는 데 가장 큰 역할을 할 수 있을 것으로 생각된다. 이후 $LaAlO_3/Sr_{0.5}Ca_{0.5}TiO_3/SrTiO_3$ 와 같은 다른 복합 시스템에서도 이와 같은 방법론을 적용하는 방식으로 후속 연구를 진행하여 이에 대하여 일반화를 시키고자 한다.

주요어 : 이차원 전자 가스, 구면 수차보정 투과전자현미경, 팔면체 틀어짐 각도, 페로브스카이트 산화물

학번 : 2013-20605